Search for W and Z Bosons in $\overline{p}p \rightarrow 2$ jets $+ \gamma$ at $\sqrt{s} = 1.8$ TeV

M. Brozović, A.T. Goshaw, M. Kruse, W.J. Robertson

February 4, 2005

Abstract

We present a study of the dijet invariant mass distribution for the process $\overline{p}p \rightarrow 2$ jets$+\gamma + X$, at a center of mass energy of 1.8 TeV, using data collected by the CDF experiment. We compare the data to predictions of tree level QCD calculations of the production of a photon with two jets, together with the resonant processes $\overline{p}p \rightarrow W/Z+\gamma+X$, in which the W and Z bosons decay hadronically. A fit is made to the dijet invariant mass distribution combining the non-resonant background and resonant processes. We use the result to establish a limit for the inclusive production cross section of $W/Z+\gamma$ with hadronic decay of the W and Z bosons.

1 INTRODUCTION

The production of final states containing W or Z bosons in association with a photon (γ) in $\overline{p}p$ collisions at $\sqrt{s} = 1.8$ TeV has been studied by the CDF and DØ collaborations using event samples in which the W and Z bosons decay to leptons [1]. Identification of $W\gamma$ and $Z\gamma$ events in which the W/Z decay hadronically is experimentally difficult because of large background from direct production of 2 jet + γ and three-jet events. A study of the general kinematic characteristics of 2 jet + γ production has been conducted using 16 pb^{-1} of data from CDF Run 1a, however the characteristics of the dijet invariant mass distribution were not investigated [2].

We examine events with two jets and a high transverse energy photon for evidence of $\gamma + W/Z \to q\overline{q}$ final states. We fit the dijet invariant mass distribution to a mixture of boson resonance decay and QCD background. The methods established in this analysis [3] could prove useful for identifying similar signals coming from $X \to jj$ decay which are embedded in large QCD background. In this study we analyze 2 jet + γ events from 90 pb^{-1} of $\overline{p}p$ data, collected with the CDF detector during Run 1b of the Tevatron, recorded by requiring a photon candidate with electromagnetic transverse energy greater than 23 GeV.

We use leading order (LO) event generators and a detector response simulation to characterize $W\gamma$ and $Z\gamma$ production, and to represent the background contributions from 2 jet + γ production and 3 jet production, in which one of the jets is misidentified as a photon.

2 THE DETECTOR

A comprehensive description of the Collider Detector at Fermilab (CDF) may be found in [4]. We use a coordinate system with z along the proton beam, azimuthal angle ϕ, polar angle θ, and pseudo-rapidity $\eta = -\ln\tan(\theta/2)$. The transverse energy of a particle (e.g. photon, electron, jet) is defined as $E_T = E\sin\theta$. The primary components relevant to this analysis are those that measure jet energies and positions and photon energies, positions and profiles, and those that establish the $\overline{p}p$ interaction vertex.

The central tracking chamber (CTC) and vertex tracking chamber (VTX) are used to establish the interaction z position using charged tracks associated with jets. The CTC is a jet-cell drift chamber which provides space point information used to measure the momentum of charged particles. It covers a rapidity range of $|\eta| < 1.2$. The VTX is a time projection chamber positioned between the beam pipe and the CTC that provides improved interaction vertex measurement with the extrapolation of tracks reconstructed in the CTC.

Scintillator-based electromagnetic (CEM) and hadronic (CHA) calorimeters in the central region ($|\eta| \leq 1.1$) are arranged in projective towers of size $\Delta\eta \times \Delta\phi \approx 0.1 \times 0.26$. The end-wall hadronic calorimeter (WHA) and the end-plug electromagnetic (PEM) and hadronic (PHA) calorimeters extend the rapidity coverage out to $|\eta| \leq 2.4$.

Two additional detector elements are used for photon identification. The central strip chambers (CES) are multi-wire proportional chambers with segmented cathode strips. They are located near the shower maximum of the central electromagnetic detector. The anode wires measure ϕ and the cathode strips measure η for showers in the CEM. The central preradiator (CPR) is a set of multi-wire proportional chambers, positioned between the magnet solenoid and the CEM, used to measure the shower pulse heights of electron-positron pairs from photons converting in a solenoid of thickness 1.1 radiation lengths. They provide discrimination between single photons and multi-photon showers arising from π^0 and η decays.

3 EVENT SELECTION

Events with photon candidates were selected using a trigger which required a high threshold of energy deposited in the central electromagnetic calorimeter. Photon clusters were reconstructed by combining the energy from neighboring CEM cells with a seed cell having energy above a threshold of 3 GeV. A photon candidate was required to have clustered energy $E_T > 23$ GeV.

In the offline data analysis, the measured photon energies were corrected using a CDF algorithm [5] which takes into account variations of CEM response within a cell, cell-to-cell energy sharing, and a global transverse energy scale. A photon candidate was required to be isolated, with less than 15% additional energy ($E_{CEM} + E_{CHA}$) within a cone of radius $\Delta R = \sqrt{\Delta\phi^2 + \Delta\eta^2}$ centered on the photon direction. In order to reject electrons, a tracking isolation requirement was imposed by summing the transverse momentum of tracks within the 0.4 cone around the photon direction. The sum of p_T of the tracks was required to be less that 2 GeV/c.

The trigger efficiency for photon candidates has been measured in the data as a function of the photon transverse momentum. The trigger threshold curve, used in acceptance calculations, is shown in Figure 1.

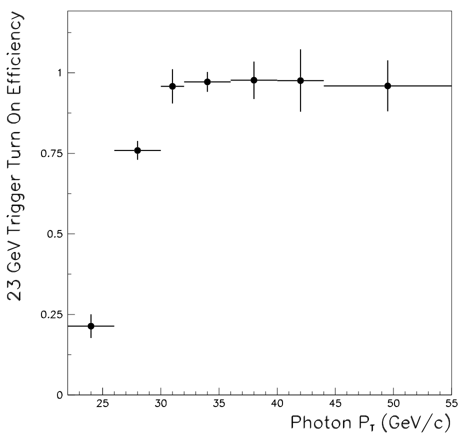

Figure 1: The 23 GeV isolated photon trigger efficiency [6]. The efficiency plateaus at 0.970 ± 0.006.

The ratio of the energy deposited in the hadronic calorimeter (E_{HAD}) to the energy deposited in the electromagnetic calorimeter (E_{CEM}) for a photon candidate passing the above cuts must satisfy the requirement

$$\frac{E_{HAD}}{E_{CEM}} \leq 0.055 + 0.00045 E(\gamma),$$

with $E(\gamma)$ in GeV.

Typically, for a photon, the above ratio is less than 10%. A lateral sharing parameter for CEM clusters measures the spread of energy over calorimeter cells adjacent to the seed cell, and selects photons based upon the spread expected from measurements in an electron test beam.

The photons had to pass fiducial cuts that require sufficient shower containment in the CES chambers. The highest energy strip cluster and the highest energy wire cluster were chosen to determine the position and transverse profile of a photon candidate. Any additional clusters in the CES within the boundaries of the calorimeter energy cluster had to have energy less than 2.39 GeV + 0.01 $E_T(\gamma)$ GeV.

Multi-photon backgrounds from π^0 and η decays are suppressed by requiring the transverse profile of the shower energy observed in the CES to match to a reference profile measured an electron test beam. A partial separation of direct photons from multi-photon backgrounds was made based on the quality of the shower shape agreement. Additional details of the photon cuts may be found in [7].

The energy from identified photons is removed from the calorimeter cells and the remaining energy is clustered to reconstruct jets. Hadronic jets are identified using a cone clustering algorithm, which is described in detail elsewhere [8]. Jets clustered with a cone size of 0.7 had their energies corrected for calorimeter nonlinearity and cell-to-cell non-uniformity. An underlying event correction takes into account energy deposition from particles not associated with the parent parton falling within the jet clustering cone, and an out-of-cone correction accounts for energy from the jet which is radiated outside the jet clustering cone.

The sample of events with exactly two jets having E_T greater than 15 GeV and $|\eta| \leq 1.1$ is used. The rapidity cutoff insures that the reconstruction efficiency for tracks associated with these jets is uniform. Any additional jets present in the event within $|\eta| < 2.4$ must have $E_T \leq 10$ GeV. Each of the two central jets must include at least one valid beam-constrained track, which is used to calculate the jet vertex position. The vertices determined from the tracking information from the two jets in an event must lie within 10 cm of each other. This cut removes instances of jets from different $p\bar{p}$ collisions during the same beam-crossing being counted as a single interaction. The interaction vertex is taken to be the average of the two jet vertices and must lie within 60 cm of the center of the detector. This vertex, together with the information from the CES, is used to define the photon trajectory.

A total of approximately 2.7 million triggered events were recorded. A sample of 9493 events satisfied all photon and jet selection criteria. The photon E_T distribution is shown in Figure 2. Figure 3 shows the E_T and η distributions for the two leading jets in the event, ordered by E_T. The most energetic jet has average E_T of 43 GeV, while the second jet has average E_T of 25 GeV. A plot of the dijet invariant mass distribution is shown in Figure 4.

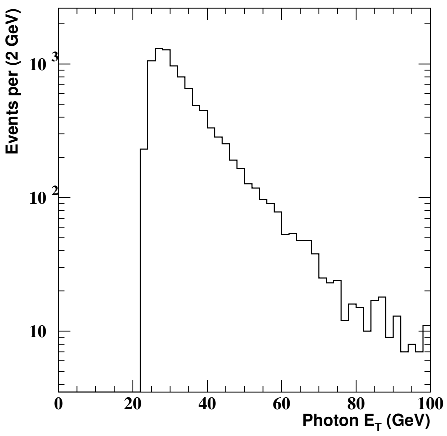

Figure 2: Photon E_T Distribution from γ + 2 jet events.

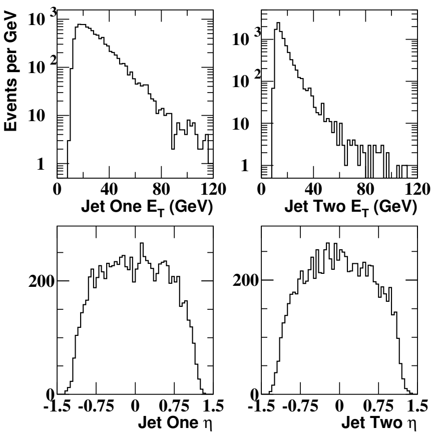

Figure 3: The E_T and η distributions for the two leading jets.

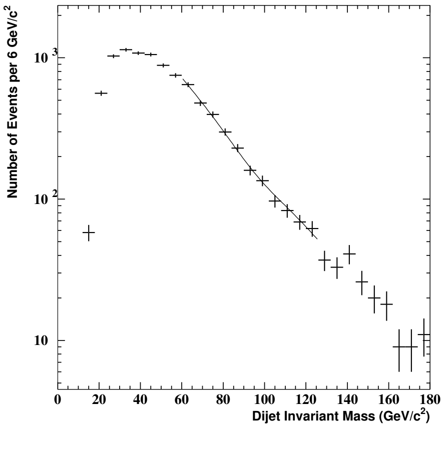

Figure 4: Dijet mass spectrum from 2 jet + γ data. There are 2656 events in the m_{jj} region from 60 to 126 GeV/c^2. The solid fit corresponds to the background + signal fit as described in Section 6.

4 EVENT GENERATION AND SIMULATION

There are several physical processes which produce the 2 jet + photon final state. Our primary study is the resonant $W/Z\gamma$ production with W/Z decaying to jets. In addition to these signal events, we also generate two QCD backgrounds which contribute to the two-jet + photon data sample. The first is non-resonant two-jet + photon production and the second is three-jet production. In the latter, we further select events which have one of the jets misidentified as a photon.

A CDF detector simulation produces event records with the same structure as the data. These generated events are then subject to the same photon and jet selection cuts, and detector geometric acceptance, as applied to the data.

4.1 Signal Simulation

The signal processes $p\bar{p} \to W + \gamma$ and $\overline{p}p \to Z + \gamma$, in which the W/Z decay to 2 jets, are modeled using a LO matrix element calculation [9], which includes contributions from initial and final state inner bremsstrahlung processes. The Monte Carlo simulation produces photons with $E_T \geq 15$ GeV and ΔR between the photon and partons greater than 0.4. We also require that the invariant mass of the quark-antiquark pair from the W/Z decay is greater than the boson mass minus three times the boson natural width. This latter cut tends to suppress final state bremsstrahlung, and produces a characteristic W/Z resonant mass peak that simulates the signal searched for in our data (see section 6). The factorization scale was set equal to the square of the colliding partons center of mass energy $\sqrt{\hat{s}}$. The MRSA$'$ parton distribution functions were used. The parton-level events are run through HERWIG for parton shower evolution and hadronization. The resulting dijet mass distributions from W and Z decay, together with the combined distribution, are shown in Figure 5.

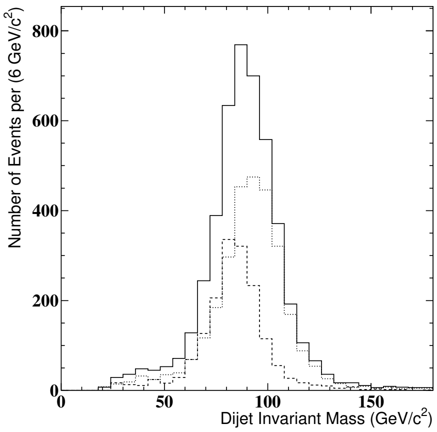

Figure 5: The invariant mass distributions of the two leading jets from the LO $W\gamma$ and $Z\gamma$ simulations, together with their sum. The dijet invariant mass m_{jj} is defined as $\sqrt{(E_1+E_2)^2-(\vec{P}_1+\vec{P}_2)^2}$, where E_i and $\vec{P}_i$ are the corrected energies and momenta of the two leading jets.

The $W\gamma$ and $Z\gamma$ signal acceptance is calculated using the Monte Carlo events generated as described above, with a full CDF detector simulation. The details of the acceptance calculations are presented in Tables 1 and 2 for the $W\gamma$ and $Z\gamma$ events respectively. The uncertainty in the acceptances for each cut were estimated by varying the upper and lower limits on the cut parameters and measuring the effects on the number of events passing the cuts. The errors in the Table 1 and Table 2 represent cumulative errors on the efficiency, where all the errors of the subsequent cuts are added in quadrature.

Table 1: Wγ Efficiencies

Wγ Sample	Events	%	Error
Generated	97298	100	
Photon $\|\eta\|$	55487	57.03	+ 2.40, –2.83
Photon ID	25939	26.67	+ 1.13, –2.02
Photon trigger	9567	9.83	+ 0.62, –0.83
Basic Jet	8186	8.41	+ 0.56, –0.72
Jet E_T	4227	4.34	+ 0.32, –0.39
Jet $\|\eta\|$+track	1677	1.72	+ 0.27, –0.28

Table 2: Zγ Efficiencies

Zγ Sample	Events	%	Error
Generated	102210	100	
Photon $\|\eta\|$	68563	67.08	+ 2.55, –3.16
Photon ID	37080	36.28	+ 1.38, –2.78
Photon trigger	15294	14.96	+ 0.86, –1.45
Basic Jet	13555	13.26	+ 0.79, –1.30
Jet E_T	6806	6.66	+ 0.44, –0.68
Jet $\|\eta\|$+track	2946	2.88	+ 0.42, –0.47

The photon η cut was varied from 1.0 to 1.2. The photon ID cut combines the number of charged tracks associated with a photon cluster, the sum of transverse momenta p_T of the charged tracks, and the photon isolation. The number of charged tracks allowed in a photon cluster cone was varied from zero to two. The effect of this change was propagated through to the photon isolation cuts, and the resulting variation in the acceptance was used as an estimate of the systematic uncertainty in the photon identification. Finally, we estimated the uncertainty in the acceptance due to the photon trigger. The key threshold points in the turn-on function shown in Figure 1 were varied by $\pm5\%$ from the nominal value. For example, the photons with 23 GeV $\leq E_T \leq$ 26 GeV originally had 22% probability to pass the trigger. The high acceptance cut lowers this probability to 17%, while the low acceptance cut raises this probability to 27%. The resulting effect on the acceptance was taken as a systematic uncertainty. Tables 1 and 2 summarize the photon selection efficiencies and their uncertainties.

The basic jet cut includes the requirement that there be at least two jets with $E_T > 10$ GeV and $|\eta| < 2.4$. The E_T cut was varied from 9.5 to 10.5 GeV and the $|\eta|$ cut was varied from 2.3 to 2.5. The jet E_T cut requires exactly two jets with $E_T > 15$ GeV. The jet E_T cut was varied from 14 to 16 GeV and the jet η selection varied from $|\eta| < 1.0$ to $|\eta| < 1.2$. Tables 1 and 2 summarize the selection efficiencies with their uncertainties due to these jet selection cuts. The final overall event selection efficiency for $W\gamma$ events is $0.0172^{+0.0027}_{-0.0028}$ and for $Z\gamma$ events $0.0288^{+0.0042}_{-0.0047}$.

4.2 Background Simulation

We use a tree level calculation for the $\gamma + 2$ jets background process which includes both prompt photon and bremsstrahlung contributions [10], followed by HERWIG for parton evolution and fragmentation [11]. In addition, three-jet events are generated using PYTHIA [12], with JETSET preforming the parton evolution and fragmentation. Based on the "jet–fakes–photon" probability distribution measured from jet data, each of the three leading jets are checked for being mis–identifed as a fake photon. A jet with $E_T \geq 23$ GeV has a maximum probability of 8×10^{-4} to fake a photon.

The di-jet mass distribution from the data favors a background mixture of 60% two-jet+photon and 40% three-jet in which one jet fakes a photon. Figure 6 shows the di-jet mass distribution for this combination of backgrounds. For masses between 60 GeV/c^2 and 126 GeV/c^2 the background distribution is fit well to the form $dN/dm_{jj} = A\exp(-bm_{jj})$ as shown by the solid line in Figure 6. This slope is known to be affected by the inclusion of higher-order QCD contributions, so we leave the exponential slope of the background as a free parameter in the fit to the experimental dijet mass mass spectrum to a combination of signal plus background (see section 6 for details).

5 STANDARD MODEL PREDICTIONS FOR $W\gamma$, $Z\gamma$ CROSS SECTIONS

Four parton–level event samples were generated using the procedure described in section 4.1: $W^+\gamma$ (where $W^+ \to u\bar{d}$), $W^-\gamma$ (where $W^- \to d\bar{u}$), $Z\gamma$ (where $Z \to u\bar{u}$), and $Z\gamma$ (where $Z \to d\bar{d}$). Partons are treated as massless in the model. In order to include the W/Z decays to heavy quarks, the initial "light" cross sections are multiplied by appropriate factors. For example, $W^+ \to u\bar{d}$ is multiplied by 2.1 to account for $c\bar{s}$, $c\bar{d}$, $u\bar{s}$ and $c\bar{b}$ decays. The same is valid for the $W^- \to d\bar{u}$. The cross section for $Z \to u\bar{u}$ is multiplied by 2.0 to account for $Z \to c\bar{c}$, while the cross section for $Z \to d\bar{d}$ is multiplied by factor 3.0 to include $Z \to s\bar{s}$, $b\bar{b}$ decays. In addition, the final cross sections

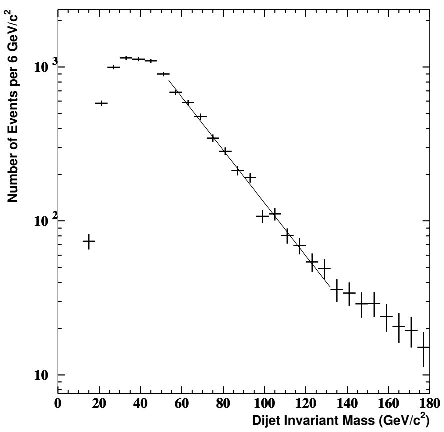

Figure 6: Combined background of two-jet + γ events and three-jet events in which one jet is identified as a photon. The distributions are mixed in the ratio 60% to 40%. The exponential fit is presented with a solid line.

are multiplied by a factor of 1.3 [13] to take into account higher order QCD corrections.

The resulting cross section for $p\bar{p} \rightarrow W^{\pm} + \gamma$ with $W^{\pm}$ decay to quark-antiquark is 6.35 pb, and for $p\bar{p} \rightarrow Z + \gamma$ with the Z decay to quark-antiquark is 6.5 pb. These are for events generated with $E_T(\gamma) \geq 15$ GeV, $\Delta R(\gamma - q) > 0.4$ and the quark-antiquark mass greater than the boson mass minus three times the boson natural width.

With an integrated luminosity of 90 pb^{-1} we would expect $N_{W\gamma} = 90 \times 6.35 \times 0.017 = 10^{+1}_{-2}$ events, and $N_{Z\gamma} = 90 \times 6.5 \times 0.029 = 17^{+2}_{-2}$ events. The total is approximately 27 events in the two-jet + photon data sample in the dijet invariant mass region between 60 and 126 GeV/c^2. The generated $W^{\pm}\gamma$ and $Z\gamma$ events are combined in proportion to the calculated process cross sections.

The dijet mass distribution from the combined $W/Z\gamma$ generated events shown Figure 5 is normalized to a total area of one and fit to a double Gaussian

$$\frac{1}{N}\frac{dN}{dm_{jj}} = S(m_{jj})$$

$$S(m_{jj}) = S_1 e^{-\frac{(m_{jj}-m_1)^2}{(2\sigma_1)^2}} + S_2 e^{-\frac{(m_{jj}-m_2)^2}{(2\sigma_2)^2}}$$

The fit parameters are $S_1 = 0.028$ (GeV/c^2)$^{-1}$, $m_1 = 89.6$ GeV/c^2, $\sigma_1 = 12.5$ GeV/c^2, and $S_2 = 0.002$ (GeV/c^2)$^{-1}$, $m_2 = 76.3$ GeV/c^2, $\sigma_2 = 41$ GeV/c^2. These parameters are used in fitting the dijet mass distribution from the data to a combination of an exponential background and the signal distributions.

The widths of the invariant mass spectra for simulation of W and Z production shown in Figure 5 are consistent with a mass resolution determination from a previous study of inclusive two jet production at CDF [14]. Over the dijet mass range from 60 to 126 GeV/c^2 the fractional dijet mass resolution ($\delta_{m_{jj}}/m_{jj}$) is essentially constant at 15%.

6 FITTING STANDARD MODEL PREDICTIONS TO THE DATA

A sum of predicted background and resonant dijet mass distributions is fit to a histogram of the data in 11 bins over the mass range 60 to 126 GeV/c^2. The fitting procedure involves maximizing the likelihood function:

$$L = \exp(-\chi^2/2)$$

where the χ^2 is given by

$$\chi^2(\tilde{f}, \tilde{b}) = \sum_{i=1}^{n} \frac{(N_i - \tilde{N}_i(\tilde{f}, \tilde{b}))^2}{\sigma_i^2}$$

The optimal set of the two free parameters $(\tilde{f}, \tilde{b})$ is found by minimizing the χ^2 of the fit to the dijet mass distribution of the data. N_i and σ_i are the number of events in the ith mass bin of the data, and the statistical error. The total number of events in the mass range from 60-126 GeV/c^2 is $N_o = 2594$. The data distribution $d\tilde{N}/dm_{jj}$ is described by a combination of background (B) and resonant W/Z signal (S).

$$\frac{d\tilde{N}}{dm_{jj}} = N_o((1-\tilde{f})B(m_{jj}, \tilde{b}) + \tilde{f}S(m_{jj}))$$

Here, $\tilde{f}$ is the fraction of the signal in data and $\tilde{b}$ is the exponential slope of the background dijet mass distribution. Functions $B(m_{jj}, \tilde{b})$ and $S(m_{jj})$ represent parametrized shapes of the dijet mass spectrum for the background and the signal. The background distribution is represented by an exponential

$$B(m_{jj}, \tilde{b}) = B_o e^{\tilde{b}m_{jj}}$$

while the signal is represented by the double Gaussian distribution function $S(m_{jj})$ described above. The functions $B(m_{jj},\ \tilde{b})$ and $S(m_{jj})$ are normalized so that the area under each, over the mass range from 60 to 126 GeV, is one.

$$\int_{60}^{126} B(m_{jj}, \tilde{b}) dm_{jj} = 1$$

$$\int_{60}^{126} S(m_{jj}) dm_{jj} = 1$$

The prediction for the number of events in the ith mass bin is:

$$\tilde{N}_i(\tilde{f}, \tilde{b}) = \int_{bin\ i} \left| \frac{d\tilde{N}}{dm_{jj}} \right| dm_{jj}$$

The cross section for production of $W\gamma$ and $Z\gamma$ ($\sigma_{W/Z\gamma}$) can be expressed in terms of the fraction $\tilde{f}$

$$\tilde{\sigma}_{W/Z\gamma} = \frac{N_o \tilde{f}}{\varepsilon_{W/Z\gamma}\mathcal{L}}$$

where $\mathcal{L}$ is the total integrated luminosity = 90 ± 4 pb^{-1} [15], and $\varepsilon_{W/Z\gamma}$ is the combined $W/Z\gamma$ event detection efficiency = $0.0230^{+0.0050}_{-0.0055}$. This final efficiency is an average of $\varepsilon_{W\gamma}$ and $\varepsilon_{Z\gamma}$ quoted in Tables 1 and 2.

From the LO QCD predictions for the background and signal cross sections, we would expect about 1% of the events in the fit region of the dijet invariant mass spectrum (60 - 126 GeV/c^2) to originate from the hadronic decay of W/Z bosons. The fit that maximizes the likelihood function (minimizes the chi square) $L(\tilde{f})$ yields a value for f of -0.05 ± 0.05, corresponding to an unphysical negative cross section. This fit to the data is shown as the solid line in Figure 4.

We establish an upper limit for the $W/Z\gamma$ cross section, based on our definition of the fit likelihood function. The likelihood function is computed as a function of the $W/Z\gamma$ cross-section $L(\sigma)$.

The χ^2 minimization procedure to the data takes into account the possible effects of variations in the event efficiency and integrated luminosity. An event efficiency is selected randomly from a gaussian distribution with mean value of 0.0230 and width of 0.0050. Then an integrated luminosity is selected from a gaussian distribution with mean value of 90 pb^{-1} and width of 4 pb^{-1}. The best fit χ^2 is found, and then new values for the event efficiency and integrated luminosity are selected and the minimization procedure is repeated. The average value of the χ^2 for this sample is calculated and used to determine the likelihood value for a given cross section. The distribution of likelihood values versus cross section is shown in Figure 7.

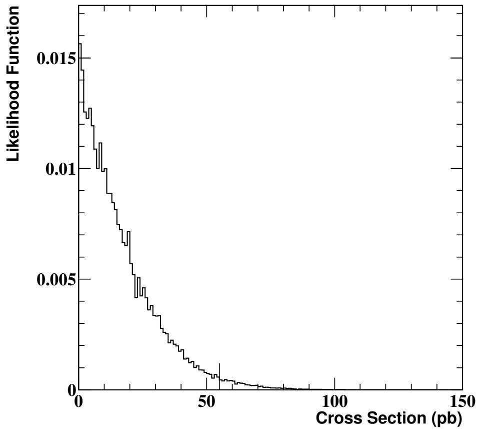

Figure 7: Likelihood function versus $\sigma_{W/Z\gamma}$ as described in the text.

By integrating the likelihood distribution from $\sigma = 0.0$ to the value at which the area under the function is 95% of the total area we find a cross section limit for $W/Z\gamma$ production. The result is $\sigma(\bar{p}p \to W\gamma) \times BR(W \to jj) + \sigma(\bar{p}p \to Z\gamma) \times BR(Z \to jj) \leq 55$ pb compared to a Standard Model expectation of 13 pb.

7 Summary

We have searched for the process $\overline{p}p \to W/Z + \gamma + X$ in which the W and Z bosons decay hadronically. The sensitivity of the search is enhanced by fitting the dijet mass spectrum from $\overline{p}p \to 2$ jet $+\gamma$ to that expected from QCD models for the background and the line shape from the $W/Z \to 2$ jets decay. The Standard Model prediction of the cross section for $\overline{p}p \to W/Z + \gamma$, with the W/Z bosons decaying to quark- antiquark pairs, is 13 pb. This cross section is for photons with of $E_T(\gamma) > 15$ GeV, $\Delta R(\gamma - q) > 0.4$ and for quark-antiquark pair masses greater than the boson mass minus three times the boson natural width.

The data from 90 pb^{-1} of $\overline{p}p$ interactions show no evidence of this process. By integrating the likelihood function we get a 95% confidence level upper limit to the cross section of 55 pb, consistent with the Standard Model prediction. This analysis method could prove effective for measuring the $W/Z \to$ dijet mass signal in this channel from a larger statistics sample of data being collected by the CDF experiment in Tevatron Run 2.

We thank the Fermilab staff and the technical staffs of the participating institutions for their vital contributions. We also thank Uli Baur and Jeff Owens for valuable discussions. This work was supported by the U.S. Department of Energy and National Science Foundation; the Italian Istituto Nazionale di Fisica Nucleare; the Ministry of Education, Culture, Sports, Science and Technology of Japan; the Natural Sciences and Engineering Research Council of Canada; the National Science Council of the Republic of China; the Swiss National Science Foundation; the A.P. Sloan Foundation; the Bundesministerium fuer Bildung und Forschung, Germany; the Korean Science and Engineering Foundation and the Korean Research Foundation; the Particle Physics and Astronomy Research Council and the Royal Society, UK; the Russian Foundation for Basic Research; the Comision Interministerial de Ciencia y Tecnologia, Spain; and in part by the European Community's Human Potential Programme under contract HPRN-CT-20002, Probe for New Physics.

References

[1] F. Abe et al, Phys. Rev. Letters **74**, **1936** (1995); F. Abe et al, Phys. Rev. Letters **74**, **1941** (1995).

[2] F. Abe et al, Phys. Rev **D57**, **67** (1998).

[3] M. Brozovic Ph.D. Thesis, Duke University, (2002)

[4] F. Abe et al, Nuclear Instruments and Methods in Physics Research **A271**, **387** (1988).

[5] F. Abe et al, Phys. Rev. Letters **77**, **438** (1996).

[6] D. Partos Ph.D. Thesis, Brandeis University, 61 (2001)

[7] F. Abe et al, Phys. Rev **D48**, **2998** (1993).

[8] F. Abe et al, Phys. Rev **D45**, **1148** (1992).

[9] U. Baur and D. Zeppenfeld, Nucl. Phys. **B308**, **127** (1988); U. Baur and E.L. Berger, Phys. Rev. **D47**, **4889** (1993).

[10] H. Baer, J. Ohnemus and J.F. Owens, Phys. Rev. **D42**, **61** (1990).

[11] G. Marchesini et al., Comp. Phys. Commun. **67**, **465** (1992).

[12] T. Sjöstrand, Comp. Phys. Commun. **82**, **127** (1988).

[13] U. Baur, private communication.

[14] F. Abe et al, Phys. Rev. **D41**, **1722** (1990).

[15] D. Cronin-Hennesy, A. Beretvas and F. Derwent, Nuclear Instruments and Methods, **A443**, **37** (2000).